PHYSICAL REVIEW B **92**, 100508(R) (2015)

Observation of two-dimensional bulk electronic states in the superconducting topological insulator heterostructure $Cu_x(PbSe)_5(Bi_2Se_3)_6$: Implications for unconventional superconductivity

K. Nakayama,[1] H. Kimizuka,[1] Y. Tanaka,[1] T. Sato,[1] S. Souma,[2] T. Takahashi,[1,2] Satoshi Sasaki,[3,*] Kouji Segawa,[3,†] and Yoichi Ando[3,‡]

[1]*Department of Physics, Tohoku University, Sendai 980-8578, Japan*

[2]*WPI Research Center, Advanced Institute for Materials Research, Tohoku University, Sendai 980-8577, Japan*

[3]*Institute of Scientific and Industrial Research, Osaka University, Ibaraki, Osaka 567-0047, Japan*

(Received 2 April 2015; published 28 September 2015)

We have performed angle-resolved photoemission spectroscopy (ARPES) on $Cu_x(PbSe)_5(Bi_2Se_3)_6$ [(CPSBS); $x = 1.47$], a superconductor derived from a topological insulator heterostructure, to elucidate the electronic states relevant to the occurrence of possible unconventional superconductivity. Upon Cu intercalation into the parent compound $(PbSe)_5(Bi_2Se_3)_6$, we observed a distinct energy shift of the bulk conduction band due to electron doping. Photon-energy-dependent ARPES measurements of CPSBS revealed that the observed bulk band forms a cylindrical electronlike Fermi surface at the Brillouin-zone center. The two-dimensional nature of the bulk electronic states puts strong constraints on the possible topological character of the superconducting state in CPSBS.

DOI: 10.1103/PhysRevB.92.100508 PACS number(s): 74.78.Fk, 73.20.−r, 75.70.Tj, 79.60.−i

Topological superconductors (TSCs) manifest a novel quantum state of matter in which the nontrivial topology of the bulk state leads to the emergence of gapless Andreev bound states often consisting of Majorana fermions [1–5]. Owing to the exotic characteristics of Majorana fermions, such as particle-antiparticle symmetry and potential use for fault-tolerant quantum computations, the search for TSCs is one of the most attractive and emergent topics in condensed-matter physics. It has been theoretically proposed that topological insulators (TIs), which are characterized by the gapless topological edge or surface states originating from a band inversion due to strong spin-orbit coupling, can provide a platform to realize topological superconductivity when enough carriers are introduced [6,7]. A first example of the superconductor derived from TIs is $Cu_xBi_2Se_3$ [8,9] in which point-contact spectroscopy experiments observed a pronounced zero-bias conductance peak indicative of unconventional surface Andreev bound states [10]. A subsequent experiment in a doped topological crystalline insulator (TCI) $Sn_{1-x}In_xTe$ [11] has also reported similar Andreev bound states. These results suggest that the carrier doping into the TIs and TCIs is an effective strategy to search for three-dimensional (3D) TSCs, whereas the electronic states (in particular, the superconducting pairing symmetry) and their relationship to possible TSC nature are still under intensive debate [9–20].

Very recently, it has been suggested that a new TI-based superconductor $Cu_x(PbSe)_5(Bi_2Se_3)_6$ (called CPSBS here) is an intriguing candidate of TSC [21]. The parent compound is the $m = 2$ phase of lead-based homologous series $(PbSe)_5(Bi_2Se_3)_{3m}$ (called PSBS) in which Bi_2Se_3 with the thickness of m quintuple layers (QLs) alternates with a bilayer PbSe unit, forming a natural multilayer heterostructure of TI (Bi_2Se_3) and an ordinary insulator (PbSe) [22–26]. An angle-resolved photoemission spectroscopy (ARPES) study has revealed two Dirac-cone states hybridized with each other, suggestive of the existence of topological interface states at the boundaries between 2-QL Bi_2Se_3 and PbSe layers [27,28]. Upon Cu intercalation into the van der Waals gap at the middle of the 2-QL Bi_2Se_3 unit, superconductivity with $T_c \sim 2.9$ K has been realized [21]. An important distinction of CPSBS from other known TI/TCI-based superconductors is that an unconventional bulk superconductivity with gap nodes is inferred from the specific-heat measurement [21]. This is intriguing because the existence of gap nodes in a strongly spin-orbit coupled superconductor would give rise to spin-split Andreev bound states that are nothing but helical Majorana fermions [10,30]. Since the topological character of the superconducting state strongly depends on the topology of Fermi surface in the normal state, it is of particular importance to establish the bulk electronic states relevant to possible unconventional superconductivity in CPSBS.

In this Rapid Communication, we report a high-resolution ARPES study of PSBS ($m = 2$) and its Cu-intercalated counterpart CPSBS. By utilizing a relatively long escape depth of photoelectrons excited by low-energy photons, we have succeeded in observing a previously unidentified intrinsic bulk band structure of the 2-QL Bi_2Se_3 unit lying deeper beneath the surface. Our most important finding is that the near-E_F bulk band responsible for the superconductivity shows a two-dimensional (2D) character, in contrast to the 3D character of bulk Bi_2Se_3. We discuss the implications of the present result in relation to the possible topological superconductivity in CPSBS.

High-quality single crystals of a parent compound PSBS ($m = 2$) were grown by a modified Bridgman method using high-purity elements Pb (99.998%), Bi (99.9999%), and Se (99.999%). The crystal quality has been greatly improved from that in the previous ARPES study of PSBS [27]; in particular,

*Present address: School of Physics and Astronomy, University of Leeds, Leeds LS2 9JT, United Kingdom.

†Present address: Department of Physics, Kyoto Sangyo University, Kyoto 603-8555, Japan.

‡Present address: Institute of Physics II, University of Cologne, Köln 50937, Germany.

we obtained single-phase crystals of $m = 2$ without detectable inclusions of the $m = 1$ phase in the x-ray diffraction analysis. Cu intercalation has been achieved by the electrochemical technique, and the superconducting transition temperature (T_c) of Cu-intercalated sample (CPSBS) was estimated to be $\sim$2.9 K by a magnetic susceptibility measurement. The Cu concentration x has been determined to be 1.47 from the mass change and the inductively coupled plasma-atomic emission spectroscopy analyses. Details of the sample preparations were described elsewhere [21]. ARPES measurements were performed with MBS-A1 and VG-Scienta SES2002 electron analyzers equipped with a xenon-plasma discharge lamp ($h\nu = 8.437$ eV) at Tohoku University and with tunable synchrotron lights of $h\nu = 13$–23 eV at the beamline BL-7U at the Ultra Violet Synchrotron Orbital Radiation Facility (UVSOR) as well as $h\nu = 60$ eV at the beamline BL-28A at Photon Factory, respectively. The energy and angular resolutions were set at 10–30 meV and 0.2°–0.3°, respectively. Samples were cleaved *in situ* along the (111) crystal plane in an ultrahigh vacuum at better than 1×10^{-10} Torr. A shiny mirrorlike surface was obtained after cleaving the samples, confirming their high quality. The Fermi level (E_F) of the samples was referenced to that of a gold film evaporated onto the sample holder.

First, we present high-resolution ARPES data measured with $h\nu = 60$ eV for pristine PSBS ($m = 2$) where we revealed the presence of two domains at the surface (named domains 1 and 2), each of which is selectively probed by scanning the position of a cleaved surface with a small incident beam spot (a diameter of $\sim$100 μm). Comparison of the energy distribution curves (EDCs) and corresponding ARPES intensity plot around the $\bar{\Gamma}$ point of the Brillouin zone in Figs. 1(a)–1(d) display a marked difference in the near-E_F band structure between the two surface domains. For domain 1, the observed band structure resembles the previous ARPES result for pristine PSBS ($m = 2$) whose surface is terminated by a 2-QL Bi_2Se_3 unit [27]. Two inner electron pockets indicated by black dots in Fig. 1(a) and black curves in Fig. 1(b) are ascribed to the quantized bulk conduction band (CB) of 2-QL Bi_2Se_3 with the Rashba splitting, whereas a pair of outer-electron and hole bands (blue dots and blue curves) represent hybridized surface and interface Dirac-cone states. On the other hand, the band structure for domain 2 shows a single parabola [Figs. 1(c) and 1(d)], which resembles the quantized CB of the topmost 1-QL Bi_2Se_3 layer for PSBS ($m = 1$) [27]. These results strongly suggest that domains 1 and 2 correspond to 2-QL and 1-QL Bi_2Se_3 terminations, respectively, as schematically illustrated in Fig. 1(e). Taking into account the single-phase ($m = 2$) nature of our crystal, the different surface terminations are naturally understood by the presence of two cleavage planes for PSBS ($m = 2$), i.e.: (i) between PbSe and Bi_2Se_3 units and (ii) between two QLs within the Bi_2Se_3 unit. We note that our growth technique for the PSBS system has been greatly improved since our original report [27], and large single-phase crystals for $m = 2$ have become regularly available [26].

Next we have performed the ARPES measurements on the Cu-intercalated counterpart (CPSBS). We found that the observed spectral feature always shows a simple parabolic band [Figs. 1(f) and 1(g)] irrespective of the incident beam

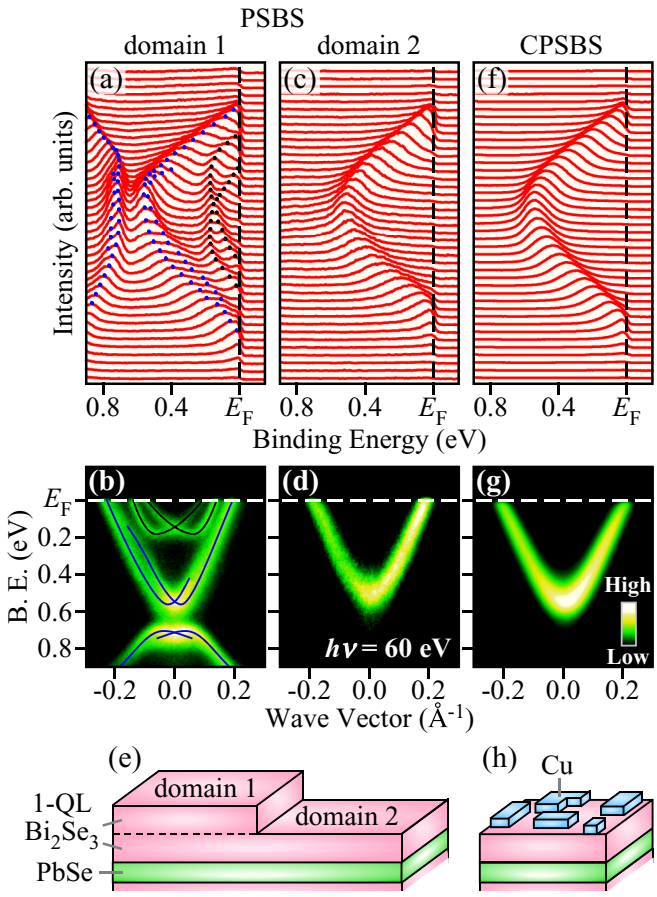

FIG. 1. (Color online) (a)–(d) Comparison of near-E_F EDCs around the $\bar{\Gamma}$ point [(a) and (c)] and corresponding ARPES intensity [(b) and (d)]. The data in (a)–(d) were taken on different domains of the cleaved surface of pristine PSBS. All the data have been obtained at $T = 30$ K with 60-eV photons. Black and blue dots in (a) [as well as black and blue curves in (b)] are a guide to the eyes to trace the dispersions of bulk conduction band and gapped Dirac-cone bands, respectively. (e) Schematic of the cleaved surface of PSBS. (f) and (g) Near-E_F EDCs and corresponding ARPES intensity plot, respectively, for CPSBS measured with $h\nu = 60$ eV. (h) Schematic of the cleaved surface of CPSBS.

position on the cleaved surface, unlike the case of PSBS. As one can immediately recognize from a side-by-side comparison of Figs. 1(d) and 1(g), the observed band dispersion for CPSBS is very similar to that for domain 2 of PSBS (except for the small downward energy shift due to electron doping). This suggests that the CPSBS sample is always cleaved at the Cu layer as illustrated in Fig. 1(h), presumably due to the expanded van der Waals gap by Cu intercalation. We thus conclude that the observed parabolic band is the quantized CB of the topmost 1-QL Bi_2Se_3 (hereafter we call CB_{1st}) partially covered with residual Cu atoms on the surface, and it may not reflect genuine bulk electronic properties. The absence of bulk electronic states (derived from the 2-QL Bi_2Se_3 unit which lies beneath the PbSe layer) at this photon energy ($h\nu = 60$ eV) is reasonable since the photoelectron escape depth ($\sim$5 Å) is much shorter than the distance between the cleaved surface and the second Bi_2Se_3 unit ($\sim$15 Å). Nevertheless, we demonstrate

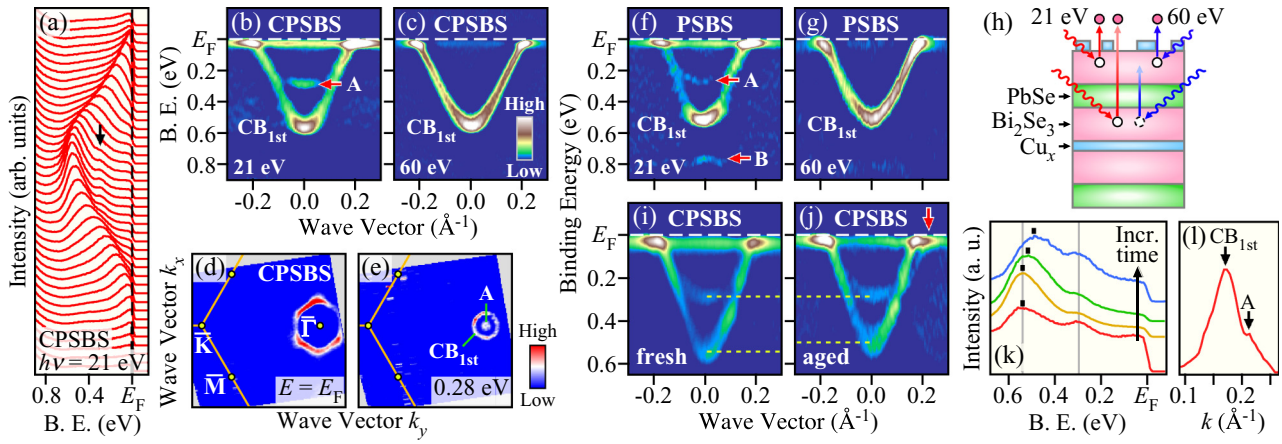

FIG. 2. (Color online) (a) EDCs around the $\bar{\Gamma}$ point for CPSBS measured at $T = 30$ K with $h\nu = 21$ eV. (b) Second-derivative intensity of (a) plotted as a function of binding energy and wave vector. (c) Same as (b), but measured with $h\nu = 60$ eV. (d) and (e) ARPES intensity map at E_F and 0.28-eV binding energy, respectively, for CPSBS plotted as a function of the in-plane wave vector. The intensity was obtained by integrating the second-derivative EDCs within ±10 meV centered at E_F or 0.28 eV. (f) and (g) Second-derivative ARPES intensity around the $\bar{\Gamma}$ point for PSBS at $h\nu = 21$ and 60 eV, respectively. (h) Schematic of the photoemission process for $h\nu = 21$ and 60 eV. (i) and (j) Near-E_F band dispersions obtained soon after cleaving and ∼10 h after cleaving, respectively, at $h\nu = 15$ eV. (k) Comparison of the EDCs at the $\bar{\Gamma}$ point for fresh and aged surfaces of CPSBS. (l) Momentum distribution curve at E_F extracted from the raw ARPES intensity of (j). Arrows indicate the Fermi wave vectors of CB_{1st} and band A.

in the following that the utilization of lower-energy photons ($h\nu = 8.4$–23 eV), which have a relatively long photoelectron escape depth (10–50 Å), allows us to investigate more intrinsic bulk electronic states of the 2-QL Bi_2Se_3 unit.

Figures 2(a) and 2(b) display the EDCs of CPSBS and corresponding second-derivative intensity plots, respectively, measured with $h\nu = 21$ eV. In addition to CB_{1st}, one can find another band at a binding energy of ∼0.28 eV (labeled A), which was not clearly visible with $h\nu = 60$ eV [Fig. 2(c)]. This band displays an electronlike dispersion around the $\bar{\Gamma}$ point along both $\bar{\Gamma}\bar{M}$ and $\bar{\Gamma}\bar{K}$ cuts [see the Supplemental Material [31] and Fig. 2(i)] and merges to CB_{1st} with approaching E_F (this point will be clarified by the surface aging measurement as shown later). This can be also recognized from the ARPES intensity mappings as a function of a 2D wave vector [Figs. 2(d) and 2(e)] where two well-separated circular intensity profiles at 0.28 eV merge to form a hexagonal Fermi surface at E_F. As shown in Fig. 2(f), we also find a similar electronlike band with $h\nu = 21$ eV at domain 2 of PSBS together with a holelike band (labeled B), both of which are not seen in the ARPES data for $h\nu = 60$ eV [Fig. 2(g)]. Since the photoelectron escape depth for $h\nu = 21$ eV is longer than that for 60 eV as schematically illustrated in Fig. 2(h), it is natural to ascribe bands A and B to the electronic states of the 2-QL Bi_2Se_3 unit located deeper beneath the surface (note that the appearance of these bands is not due to the photoionization cross section, final-state effects, k_z dispersion, or resolution effects [32]). As shown in Figs. 2(i)–2(k), the surface aging leads to a clear upward shift of CB_{1st} in contrast to the stationary nature of band A, indicating that band A is insensitive to the surface chemical environment as expected for the bulk electronic states. Thanks to the energy shift of CB_{1st}, the E_F crossing of band A is now clearly visible as marked by the red arrow in Fig. 2(j) [see also Fig. 2(l) where the momentum distribution curve at E_F contains two peaks originating from the E_F crossings of CB_{1st} and band A]. We have confirmed the E_F crossing of band A with different experimental conditions (see the Supplemental Material [31]). All these observations support the second 2-QL Bi_2Se_3 origin of bands A and B.

Having established the bulk origin of bands A and B, the next question is their band assignment. In this regard, it is useful to compare their energy dispersions with those for domain 1 of PSBS since both originate from the 2-QL Bi_2Se_3 unit. As shown in Fig. 2(f), the energy separation between the bottom of the electronlike band A and the top of the holelike band B is 0.5 eV. This value is in good agreement with an energy separation between the quantized bulk CB and the lower branch of the gapped Dirac-cone state in the topmost 2-QL Bi_2Se_3 of PSBS in Fig. 1(a). Thus, bands A and B are attributed to the quantized bulk CB and the lower branch of the gapped Dirac-cone state, respectively. It is noted that bands A and B in Fig. 2(f) are shifted downward by ∼0.1 eV as compared to those in Fig. 1(a). This may be due to the weakened band-bending effect (i.e., weakened out-of-plane potential gradient) at the second Bi_2Se_3 unit, which may also explain the absence of a clear Rashba splitting for band A in Figs. 2(b) and 2(f). Also, the absence of the upper branch of the gapped Dirac-cone state is likely due to overlapping by CB_{1st} with a dominant intensity.

To elucidate the Fermi-surface topology in the 3D momentum space relevant to the possible unconventional superconductivity of CPSBS, we have performed $h\nu$-dependent ARPES measurements by focusing on band A (hereafter we call CB_{2nd}). As one can see in the representative second-derivative intensity plots in Fig. 3(a), we commonly see CB_{2nd} and CB_{1st} over a wide $h\nu$ range of 8.4–23 eV (note that 8.4-eV photons are most bulk sensitive). A direct comparison of the EDC at the $\bar{\Gamma}$ point in Fig. 3(b) measured with various photon energies reveals that the energy position of CB_{2nd}

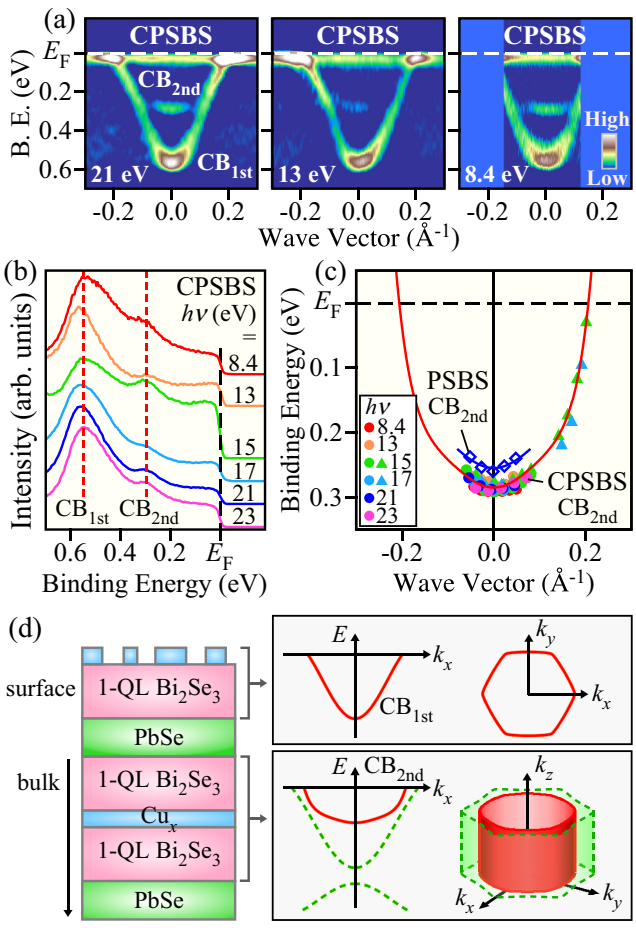

FIG. 3. (Color online) (a) Second-derivative ARPES intensity around the $\bar{\Gamma}$ point for CPSBS at various photon energies plotted as a function of binding energy and wave vector. CB_{1st} and CB_{2nd} denote the conduction bands stemming from the topmost 1-QL Bi_2Se_3 unit and the second Bi_2Se_3 unit located beneath the PbSe layer, respectively. (b) Comparison of the EDC at the $\bar{\Gamma}$ point measured with various photon energies. (c) Photon-energy dependence of the band dispersion for CB_{2nd} in CPSBS extracted from the second-derivative intensities. Filled circles and triangles represent the results for the fresh and aged surfaces, respectively. Detailed procedures used to extract the data points for the aged surface are presented in Figs. 2(j)–2(l) and the Supplemental Material [31]. The red curve is a guide for the eyes to trace the band dispersion. The band dispersion for PSBS measured with $h\nu = 21$ eV is also plotted by open diamonds. (d) Schematic of the band dispersion and the Fermi surface in the topmost and the second Bi_2Se_3 units in CPSBS.

(and CB_{1st}) is stationary with the $h\nu$ variation in contrast to the 3D-like CB of bulk Bi_2Se_3 [33]. Indeed, the extracted band dispersions of CB_{2nd} overlap very well with each other within the experimental uncertainty irrespective of the $h\nu$ value [Fig. 3(c)], demonstrating the 2D nature of CB_{2nd}. We also clarified a finite energy shift ($\sim$30 meV) of CB_{2nd} upon Cu intercalation [see Fig. 3(c)], indicating that the intercalated Cu atoms provide electrons to the Bi_2Se_3 layers, in line with the Hall-coefficient measurements [21]. Based on the present ARPES results, we show in Fig. 3(d) the schematic of the electronic structure in CPSBS. Although the topmost 1-QL Bi_2Se_3 produces a single parabolic band (CB_{1st}) localized at the surface, the bulk electronic states are confined within the 2-QL Bi_2Se_3 unit sandwiched by the insulating PbSe layers and form a cylindrical Fermi surface at the Brillouin-zone center [as shown in red in the right bottom panel of Fig. 3(d)], possibly hybridized with the topological interface state (green dashed curves). It is noted though that the topological interface state is not clearly seen in the present experiment, presumably due to its fairly weak intensity or a possible change in the band parity in the 2-QL Bi_2Se_3 unit upon Cu intercalation.

Now we discuss the implications of our results in relation to topological superconductivity. The most important finding of the present Rapid Communication is that the unconventional superconductivity in CPSBS originates from 2D bulk electronic states. Although the Fermi surface in the normal state must enclose an odd number of time-reversal invariant (TRI) momenta to realize TRI 3D topological superconductivity [6,7], the observed 2D Fermi surface in CPSBS encloses two TRI momenta (Γ and Z points). This excludes the 3D-TSC scenario. The realization of TRI 2D topological superconductivity on the top surface via the superconducting proximity effect [1–5] is also unlikely since the topological Dirac-cone states do not appear on the cleaved surface of CPSBS due to termination with trivial 1-QL Bi_2Se_3. It is noted though that CPSBS still has a chance to be a topological superconductor because of the possible occurrence of nodal superconductivity inferred from a recent specific-heat measurement [21]. According to the previous theoretical studies for $Cu_xBi_2Se_3$ with the rhombohedral D_{3d} crystalline symmetry, the appearance of gap nodes is restricted to the odd-parity E_u pairing states when the 2D Fermi surface is realized [34]. Assuming that the theoretical model proposed for $Cu_xBi_2Se_3$ is also applicable to CPSBS, the observed 2D cylindrical Fermi surface would support the odd-parity E_u pairing in CPSBS. It should be noted, however, that the crystal structure of CPSBS has the C_{2h} point-group symmetry due to the presence of the PbSe layer with square symmetry, unlike the D_{3d} symmetry of $Cu_xBi_2Se_3$. The different crystal symmetries may favor unconventional nodal pairing that was not discussed in $Cu_xBi_2Se_3$. Indeed, a recent theoretical study for CPSBS suggested that d-wave superconductivity could emerge in the case of the 2D Fermi surface [35]. In this regard, the present result is compatible with the realization of either the odd-parity E_u pairing or the even-parity d-wave pairing. Both states give rise to vertical line nodes in agreement with the temperature dependence of electronic specific heat [21]. When vertical line nodes are realized on the 2D Fermi surface of a strongly spin-orbit coupled superconductor, spin-split Andreev bound states, which are the hallmark of topological superconductivity, would emerge on some side surfaces that are perpendicular to the (111) crystal plane. Therefore, the superconducting state of CPSBS may provide an intriguing platform to explore Majorana fermions if nodal superconductivity is indeed realized. To gain further insight into the topological character, the verification of the nodal superconductivity by phase-sensitive measurements would be of particular importance. Elucidating the role of the topological interface state in the unconventional superconductivity of CPSBS is an important future task worth challenging.

In conclusion, we have reported high-resolution ARPES results on CPSBS to elucidate the band structure relevant to the unconventional superconductivity with possible nodes in the gap function. By utilizing tunable low-energy photons, we have succeeded in separately determining the band dispersion of the 1-QL Bi_2Se_3 unit at the topmost surface and that of the 2-QL Bi_2Se_3 unit lying in the bulk. The obtained bulk band structure gives evidence for the formation of a cylindrical Fermi surface in CPSBS. The present result puts strong constraints on the possible topological character of the superconducting state in CPSBS.

We thank T. Toba for his help with the crystal growth. We also thank T. Shoman, H. Kumigashira, K. Ono, M. Matsunami, and S. Kimura for their assistance with the ARPES measurements. This work was supported by JSPS (Grants No. KAKENHI 23224010, No. 26287071, No. 15H02105, No. 25287079, No. 24540320, and No. 25220708 and Grant-in-Aid for JSPS Fellows Grant No. 23.4376), MEXT of Japan (Innovative Area "Topological Materials Science"), AFOSR (Grant No. AOARD 124038), Inamori Foundation, the Murata Science Foundation, KEK-PF (Proposals No. 2012S2-001 and No. 2015S2-002), and UVSOR (Proposal No. 24-536).

[1] M. Z. Hasan and C. L. Kane, Rev. Mod. Phys. **82**, 3045 (2010).
[2] X.-L. Qi and S.-C. Zhang, Rev. Mod. Phys. **83**, 1057 (2011).
[3] Y. Ando, J. Phys. Soc. Jpn. **82**, 102001 (2013).
[4] J. Alicea, Rep. Prog. Phys. **75**, 076501 (2012).
[5] C. W. J. Beenakker, Annu. Rev. Condens. Matter Phys. **4**, 113 (2013).
[6] L. Fu and E. Berg, Phys. Rev. Lett. **105**, 097001 (2010).
[7] M. Sato, Phys. Rev. B **81**, 220504(R) (2010).
[8] Y. S. Hor, A. J. Williams, J. G. Checkelsky, P. Roushan, J. Seo, Q. Xu, H. W. Zandbergen, A. Yazdani, N. P. Ong, and R. J. Cava, Phys. Rev. Lett. **104**, 057001 (2010).
[9] M. Kriener, K. Segawa, Z. Ren, S. Sasaki, and Y. Ando, Phys. Rev. Lett. **106**, 127004 (2011).
[10] S. Sasaki, M. Kriener, K. Segawa, K. Yada, Y. Tanaka, M. Sato, and Y. Ando, Phys. Rev. Lett. **107**, 217001 (2011).
[11] S. Sasaki, Z. Ren, A. A. Taskin, K. Segawa, L. Fu, and Y. Ando, Phys. Rev. Lett. **109**, 217004 (2012).
[12] T. Kirzhner, E. Lahoud, K. B. Chaska, Z. Salman, and A. Kanigel, Phys. Rev. B **86**, 064517 (2012).
[13] N. Levy, T. Zhang, J. Ha, F. Sharifi, A. A. Talin, Y. Kuk, and J. A. Stroscio, Phys. Rev. Lett. **110**, 117001 (2013).
[14] H. Peng, D. De, B. Lv, F. Wei, and C.-W. Chu, Phys. Rev. B **88**, 024515 (2013).
[15] L. A. Wray, S.-Y. Xu, Y. Xia, Y. S. Hor, D. Qian, A. V. Fedorov, H. Lin, A. Bansil, R. J. Cava, and M. Z. Hasan, Nat. Phys. **6**, 855 (2010).
[16] E. Lahoud, E. Maniv, M. S. Petrushevsky, M. Naamneh, A. Ribak, S. Wiedmann, L. Petaccia, Z. Salman, K. B. Chashka, Y. Dagan, and A. Kanigel, Phys. Rev. B **88**, 195107 (2013).
[17] M. Kriener, K. Segawa, S. Sasaki, and Y. Ando, Phys. Rev. B **86**, 180505(R) (2012).
[18] T. V. Bay, T. Naka, Y. K. Huang, H. Luigjes, M. S. Golden, and A. de Visser, Phys. Rev. Lett. **108**, 057001 (2012).
[19] T. Sato, Y. Tanaka, K. Nakayama, S. Souma, T. Takahashi, S. Sasaki, Z. Ren, A. A. Taskin, K. Segawa, and Y. Ando, Phys. Rev. Lett. **110**, 206804 (2013).
[20] M. Novak, S. Sasaki, M. Kriener, K. Segawa, and Y. Ando, Phys. Rev. B **88**, 140502(R) (2013).
[21] S. Sasaki, K. Segawa, and Y. Ando, Phys. Rev. B **90**, 220504(R) (2014).
[22] M. G. Kanatzidis, Acc. Chem. Res. **38**, 361 (2005).
[23] Y. Zhang, A. P. Wilkinson, P. L. Lee, S. D. Shastri, D. Shu, D.-Y. Chung, and M. G. Kanatzidis, J. Appl. Cryst. **38**, 433 (2005).
[24] L. E. Shelimova, O. G. Karpinskii, and V. S. Zemskov, Inorg. Mater. **44**, 927 (2008).
[25] L. Fang, C. C. Stoumpos, Y. Jia, A. Glatz, D. Y. Chung, H. Claus, U. Welp, W.-K. Kwok, and M. G. Kanatzidis, Phys. Rev. B **90**, 020504(R) (2014).
[26] K. Segawa, A. A. Taskin, and Y. Ando, J. Solid State Chem. **221**, 196 (2015).
[27] K. Nakayama, K. Eto, Y. Tanaka, T. Sato, S. Souma, T. Takahashi, K. Segawa, and Y. Ando, Phys. Rev. Lett. **109**, 236804 (2012).
[28] Although the interface sates are effectively encapsulated in the bulk, it can be distinguished from the genuine bulk states by the topological nature as in the case of ultrathin films [29].
[29] Y. Zhang *et al.*, Nat. Phys. **6**, 584 (2010).
[30] M. Sato and S. Fujimoto, Phys. Rev. Lett. **105**, 217001 (2010).
[31] See Supplemental Material at http://link.aps.org/supplemental/10.1103/PhysRevB.92.100508 for details of the azimuth dependence of band dispersions.
[32] The appearance of bands A and B is not due to an increase in the photoionization cross section since: (i) The intensity of these bands is expected to show a similar photon-energy dependence to that of CB_{1st} because of their similar orbital characters (Se-4p and/or Bi-6p), and (ii) the cross-sectional ratio of these orbitals is nearly constant in the $h\nu$ range of the present Rapid Communication. Also, the absence of band A at $h\nu = 60$ eV is not due to the absence of available final states nor the k_z dispersion because it is absent over a wide $h\nu$ range of 40–80 eV. Since the energy resolution is similar ($\sim$15 meV) between the measurements with 60 and 21 eV, and the observed flat dispersion around the bottom of CB_{2nd} is much wider ($\sim$0.1 Å^{-1}) than the momentum resolution ($\sim$0.013 Å^{-1}) at $h\nu = 60$ eV, the experimental resolution is not a limiting factor to observe CB_{2nd}.
[33] Y. Xia, D. Qian, D. Hsieh, L. Wray, A. Pal, H. Lin, A. Bansil, D. Grauer, Y. S. Hor, R. J. Cava, and M. Z. Hasan, Nat. Phys. **5**, 398 (2009).
[34] T. Hashimoto, K. Yada, A. Yamakage, M. Sato, and Y. Tanaka, Supercond. Sci. Technol. **27**, 104002 (2014).
[35] L. Fu (private communication).